



Teanby, N. A., Irwin, P. G. J., Moses, J. I., & Helled, R. (2020). Neptune and Uranus: ice or rock giants? *Philosophical Transactions of the Royal Society A: Mathematical, Physical and Engineering Sciences*, 378(2187). <https://doi.org/10.1098/rsta.2019.0489>

Peer reviewed version

Link to published version (if available):  
[10.1098/rsta.2019.0489](https://doi.org/10.1098/rsta.2019.0489)

[Link to publication record in Explore Bristol Research](#)  
PDF-document

This is the author accepted manuscript (AAM). The final published version (version of record) is available online via The Royal Society at <https://royalsocietypublishing.org/doi/10.1098/rsta.2019.0489> . Please refer to any applicable terms of use of the publisher.

## University of Bristol - Explore Bristol Research

### General rights

This document is made available in accordance with publisher policies. Please cite only the published version using the reference above. Full terms of use are available: <http://www.bristol.ac.uk/red/research-policy/pure/user-guides/ebr-terms/>



Article submitted to journal

**Subject Areas:**

Solar System, Planetary Interiors,  
Planetary Atmospheres, Planet  
Formation

**Keywords:**

Neptune, interior, atmosphere,  
composition

**Author for correspondence:**

N. A. Teanby

e-mail: [n.teanby@bristol.ac.uk](mailto:n.teanby@bristol.ac.uk)Neptune and Uranus: ice or  
rock giants?

N. A. Teanby<sup>1</sup>, P. G. J. Irwin<sup>2</sup>, J. I. Moses<sup>3</sup>  
and R. Helled<sup>4</sup>

<sup>1</sup>School of Earth Sciences, University of Bristol, Wills  
Memorial Building, Queens Road, Bristol, BS8 1RJ, UK

<sup>2</sup>Atmospheric, Oceanic & Planetary Physics, University  
of Oxford, Clarendon Laboratory, Parks Road, Oxford,  
OX1 3PU. UK.

<sup>3</sup>Space Science Institute, 4750 Walnut Street, Suite  
205, Boulder, CO 80301, USA.

<sup>4</sup>Institute for Computational Science, Center for  
Theoretical Astrophysics & Cosmology, University of  
Zurich, Winterthurerstr. 190, 8057, Zurich, Switzerland

Existing observations of Uranus and Neptune's fundamental physical properties can be fitted with a wide range of interior models. A key parameter in these models is the bulk rock:ice ratio and models broadly fall into ice-dominated (ice giant) and rock-dominated (rock giant) categories. Here we consider how observations of Neptune's atmospheric temperature and composition (H<sub>2</sub>, He, D/H, CO, CH<sub>4</sub>, H<sub>2</sub>O, and CS) can provide further constraints. The tropospheric CO profile in particular is highly diagnostic of interior ice content, but is also controversial, with deep values ranging from zero to 0.5 parts per million. Most existing CO profiles imply extreme O/H enrichments of >250 times solar composition, thus favouring an ice giant. However, such high O/H enrichment is not consistent with D/H observations for a fully mixed and equilibrated Neptune. CO and D/H measurements can be reconciled if there is incomplete interior mixing (ice giant) or if tropospheric CO has a solely external source and only exists in the upper troposphere (rock giant). An interior with more rock than ice is also more compatible with likely outer solar system ice sources. We primarily consider Neptune, but similar arguments apply to Uranus, which has comparable C/H and D/H enrichment, but no observed tropospheric CO. While both ice and rock dominated models are viable, we suggest a rock giant provides a more consistent match to available atmospheric observations.

## 1. Introduction

The internal structure of giant planets is key to understanding how the solar system formed and evolved over the last 4.6 billion years. While multiple spacecraft have visited Jupiter and Saturn - including the Galileo, Juno, and Cassini orbiters - the Voyager 2 flybys of Uranus in 1986 and Neptune in 1989 remain the only spacecraft visits to the icy giants. Information from a single spacecraft flyby combined with subsequent remote observations provide a fairly limited dataset in terms of constraining a planet's internal structure, but some interpretations can be inferred from Uranus and Neptune's fundamental physical properties. Voyager 2 provided the first accurate mass, radius, bulk density, and low-order gravitational harmonics for Uranus and Neptune [1-4]. Early interpretations of planetary bulk densities of  $1.3 \text{ kg m}^{-3}$  for Uranus and  $1.6 \text{ kg m}^{-3}$  for Neptune suggested interiors dominated by ices [5,6], although the non-uniqueness of constraints on the interior was considerable, and rock-dominated interiors are also possible [7-10]. The Voyager 2 data have since been reanalysed and augmented with stellar occultations and observations of the orbits of Uranus and Neptune's moons and rings to provide more stringent constraints (reviewed in [9]). While it is clear that Uranus and Neptune have a high fraction of heavy elements, with an overall metallicity mass fraction in the range 0.7-0.9 [9], it is still unclear whether rock or ice is the dominant component. Therefore, Uranus and Neptune's internal structure remains elusive despite decades of observation and modelling. Uranus and Neptune could either be rock giants or ice giants, which has important implications for both their formation and the formation of the solar system as a whole.

Voyager 2 observations of Uranus and Neptune's magnetic fields indicate highly non-dipolar structures [11-14]. Such fields may suggest dynamo action is limited to a conducting near-surface layer [15]. This additionally constrains Uranus and Neptune's interiors by requiring some kind of conducting fluid layer to support dynamo action [16]. In the case of an ice giant this could be a superionic form of water ice that exists at high temperature and pressure [17]. In the case of a rock giant, magma dynamos such as those hypothesised on super-earths, might be a possibility [18]. However, even though silica is conductive at high pressure, it is most likely to be solid at the high pressures of a planetary core [19]. Mixtures of hydrogen and silicate present in some models [20] might have lower melting points, but it is unknown if they could support dynamo action in Uranus or Neptune's interior because of the wide range of possible conditions and limited high pressure and temperature laboratory data.

Many studies have combined observations of fundamental physical properties and high-pressure thermodynamic equations of state to infer Uranus and Neptune's internal structures [6-8,21-23]. These model-data fits are highly non-unique, but can be split into two main types representing either ice giant or rock giant scenarios [8]. Here we define ice and rock giants as having a rock:ice ratio less than or greater than unity respectively. Ice giant models typically have an outer gas envelope of hydrogen and helium, an intermediate region dominated by ices, and a small core of silicates, iron, and nickel. Such models are up to 90% ice. Rock giant models also have an outer hydrogen/helium gas envelope, but have a bulk interior dominated by silicates mixed with hydrogen/helium along with some ices. These models are up to 70% rock. An ice giant interpretation is currently favoured in the literature. However, an important source of uncertainty is that interiors dominated by rock mixed with light elements such as hydrogen have a similar density to ice mixtures, so could also fit the observed physical properties [5,8]. An additional complication is that, while simple models with distinct layers are appealing, they are not required to fit the observations. Recent work shows there may be significant mixing near internal interfaces, leading to more continuous density profiles [9,20,22]. This widens the range of possible internal structures significantly and leaves open the question of whether silicate-gas mixtures or ice mixtures dominate Uranus and Neptune's interiors [9,24-26].

In summary, there are a wide suite of interior models for Uranus and Neptune, both ice- and rock-dominated, with sharp or gradual layer transitions, but none are definitively preferred by observations of fundamental physical properties. This is severely unconstrained - even by

planetary science standards - and leaves both Uranus and Neptune's origin and the evolution of the outer solar system open to rampant speculation. This uncertainty is one of the major motivations for a new ice giant mission [27–30]. In this review we take an alternative approach by considering if atmospheric observations can provide further insight into internal structure. For Uranus, the atmospheric observations provide less of a constraint than on Neptune as there are currently no detections of tropospheric carbon monoxide on Uranus [31], which is an important part of the ice-giant case. Therefore, we primarily focus on Neptune in this review, but revisit Uranus briefly in the discussion.

## 2. Atmospheric observations and implications

Here we consider what can be inferred about Neptune's interior from atmospheric remote sensing of the outermost gas envelope layer; either from spacecraft, space-telescopes, or ground-based observatories. Low frequency radio and microwave observations have the ability to probe deepest in the atmosphere. For example, ground based measurements at centimetre wavelengths with the VLA at can probe down to 10's of bars [32,33] and Juno's microwave radiometer observations of Jupiter are sensitive to pressures of up to 1 kbar [34]. These measurements constrain the deep abundances of  $\text{NH}_3$ ,  $\text{H}_2\text{S}$ , and  $\text{H}_2\text{O}$ , but can contain ambiguities due to limitations on current laboratory spectroscopic data, interference from synchrotron emission, non-uniqueness in the interpretation, and uncertainties in the deep temperature profile [35,36]. Observations at shorter wavelengths have less of these difficulties, but such observations are limited to pressures of less than  $\sim 10$  bar: i.e., the troposphere, stratosphere, and mesosphere. This is well above the major water cloud layer and well mixed region [26,37], so is not ideal for probing the internal structure. Nevertheless, it is what we have available, and with caution some important insights can be gained.

### (a) Temperature, thermal emission, and mixing

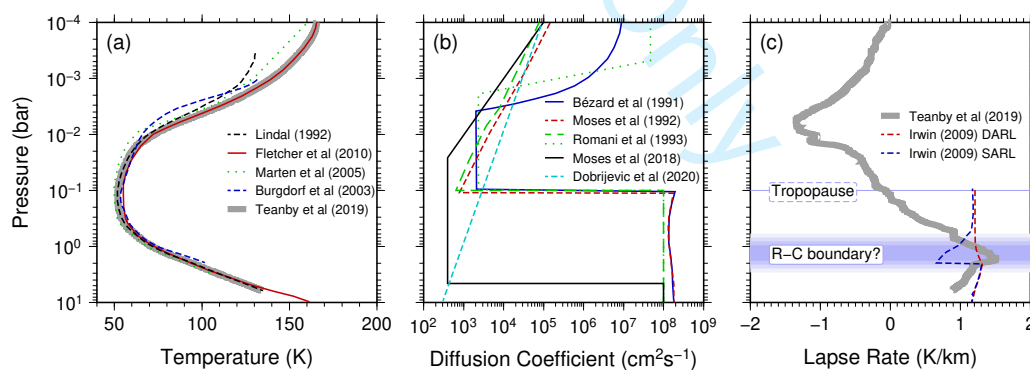


**Figure 1.** Neptune's atmosphere. (a) Temperature profiles measured by radio occultation and infra-red spectroscopy, illustrating  $\sim 5\text{K}$  uncertainty in global mean tropospheric temperature. (b) Eddy mixing profiles constrained by heat flux, composition profiles, and photochemical modelling. All photochemical models require low minimum mixing rates somewhere in the lower stratosphere or upper troposphere (0.01–1 bar), but the location of that minimum is unconstrained. This leads to variations in possible upper troposphere mixing rates of over five orders of magnitude. (c) Observed lapse rate ( $-dT/dz$ ) using a composite  $T(p)$  profile, compiled from [38] and [39] by [25], compared to the calculated lapse rate [37]. A low observed lapse rate in the upper troposphere suggests reduced mixing and a radiative convective boundary at  $\sim 1$  bar.

76 Temperature and vertical mixing are fundamental atmospheric properties and must be  
77 considered before attempting to interpret other atmospheric observations. Neptune's nominal  
78 temperature profile was determined from Voyager 2's radio occultation, covering pressures from  
79 0.35 mbar to 6.3 bar [38,40]. However, there is a degeneracy between temperature and the  
80 mean molecular mass of the atmosphere, which introduces uncertainty into the radio occultation  
81 inversion; in particular the assumed methane abundance, the He/H<sub>2</sub> ratio, and the presence  
82 of other gases such as nitrogen [40]. Neptune's rotation period is also not well constrained [9],  
83 which affects hydrostatic equilibrium calculations used in the radio occultation inversion and  
84 introduces further uncertainties [38]. Subsequently, further temperature measurements of the  
85 upper troposphere and stratosphere were inferred from infrared spectroscopic observations (for  
86 example [39,41,42]), but these suffer from low vertical resolution and also depend on the assumed  
87 atmospheric composition. A comparison between different studies reveals an uncertainty in the  
88 temperature profile of around 5 K [43,44]. Figure 1a compares various nominal temperature  
89 profiles and shows the ~5 K variation. There is also evidence for temperature variations with  
90 latitude due to differences in insolation and circulation, particularly at the poles [45].

91 Total emitted flux measurements show that Neptune emits ~2.6 times the energy it receives  
92 from the Sun [46]. This is the highest of any planet in the solar system and requires a  
93 significant internal heat source driving vigorous convection up to the observable layers. The  
94 high energy emission can be used to estimate the vertical eddy diffusion coefficient  $K_z$   
95 from mixing length theory; implying  $K_z \sim 10^8 \text{ cm}^2 \text{ s}^{-1}$  in the troposphere [44,47]. However,  
96 as the condensable species on Neptune have a higher molar mass than the surrounding  
97 atmosphere, it is possible that inhibition of moist convection could occur at pressure levels  
98 where condensation is active. For example, in the methane condensation region (~1–2 bar), and  
99 also deeper where water condenses (~100–1000 bar) [48–50]. Mixing in the upper atmosphere  
100 can be constrained to  $\sim 2\text{--}50 \times 10^6 \text{ cm}^2 \text{ s}^{-1}$  from hydrocarbon vertical profiles retrieved from the  
101 Voyager ultraviolet occultations [51,52] and from Voyager ultraviolet emission observations of  
102 the helium 584 Å line [53]. Between the upper atmosphere and lower stratosphere, mixing can  
103 be inferred by comparing observed hydrocarbon profiles to those predicted by photochemical  
104 models [52,54–57]. Numerous photochemically produced hydrocarbons have been detected in  
105 Neptune's atmosphere, including C<sub>2</sub>H<sub>2</sub>, C<sub>2</sub>H<sub>4</sub>, C<sub>2</sub>H<sub>6</sub>, C<sub>3</sub>H<sub>4</sub>, C<sub>3</sub>H<sub>8</sub>, and C<sub>4</sub>H<sub>2</sub> [37,57,58], which  
106 can be used for this purpose. Photochemical models require a relatively low eddy diffusion  
107 coefficient somewhere in the lower stratosphere or upper troposphere to prevent excessive loss  
108 of stratospheric hydrocarbons by mixing into the deep interior, but have little sensitivity to what  
109 is happening below that minimum. Figure 1b compares eddy diffusion profiles from various  
110 studies. Typically a value of  $K_z = 10^8 \text{ cm}^2 \text{ s}^{-1}$  is adopted throughout the troposphere [59], with the  
111 minimum eddy diffusion coefficient occurring in the lower stratosphere, although this is probably  
112 too gross a simplification. The most recent photochemical models arbitrarily extend the mixing  
113 minimum into the troposphere [57,60], but model results are generally not sensitive to this lower  
114 boundary condition. Therefore, mixing in the upper troposphere is currently not well constrained,  
115 either by photochemical model comparisons or the emitted heat flux.

116 Further insight into mixing can be gained by comparing the measured tropospheric lapse  
117 rate to that expected from adiabatic advection [25]. If the measured lapse rate is greater than  
118 the adiabatic lapse rate then the atmosphere can be expected to be unstable with significant  
119 mixing occurring. In the region of methane condensation (~1–2 bar), it is not currently possible  
120 to determine a precise pressure level where the temperature profile becomes super-adiabatic  
121 because of uncertainties in Neptune's methane vertical profile [48] and the co-dependence of the  
122 derived temperature profile on assumed atmospheric mean molecular mass [38,40]. However, an  
123 approximate comparison can still be made. Figure 1c compares the observed lapse rate ( $-dT/dz$ )  
124 from the composite temperature profile in [25], which is a combination of the radio occultation  
125 [38] and infra-red [39] temperature profiles, with the calculated dry adiabatic lapse rate (DALR)  
126 and saturated adiabatic lapse rate (SALR) for a H<sub>2</sub>/He/CH<sub>4</sub> atmosphere [37]. The observed lapse  
127 rate is less than both the calculated DALR and SALR for pressures below ~1 bar, indicating

1  
2  
3  
4  
5  
6  
7  
8  
9  
10  
11  
12  
13  
14  
15  
16  
17  
18  
19  
20  
21  
22  
23  
24  
25  
26  
27  
28  
29  
30  
31  
32  
33  
34  
35  
36  
37  
38  
39  
40  
41  
42  
43  
44  
45  
46  
47  
48  
49  
50  
51  
52  
53  
54  
55  
56  
57  
58  
59  
60

128 that vigorous mixing is unlikely in the uppermost troposphere ( $\sim 0.1$ – $1$  bar), no matter the  $\text{CH}_4$   
129 saturation state of the atmosphere. This suggests a radiative convective (R-C) boundary, where  
130 the majority of thermal emission originates, occurs at  $\sim 1$  bar on Neptune. This is compatible with  
131 potentially suppressed moist convection caused by methane condensation [48]. Furthermore, as  
132 noted by [25] the brightness temperature of Neptune at  $100 \mu\text{m}$  is  $\sim 60$  K [41], suggesting an  
133 emission level of  $0.5$ – $1$  bar and placing the R-C boundary at a similar level. These inferences  
134 based on lapse rate are also entirely consistent with reduced mixing in the upper troposphere as  
135 suggested by the non-detection of disequilibrium species  $\text{PH}_3$  in the upper troposphere [25].

## 136 (b) Composition

### 137 (i) He/ $\text{H}_2$

138 Neptune's observable atmosphere is primarily hydrogen and helium [61,62]. The He/ $\text{H}_2$  ratio  
139 was found to be  $0.15 \pm 0.03$  by volume for a nominal nitrogen abundance of  $0.003$  using a  
140 combination of Voyager 2 radio occultation and InfraRed Interferometer Spectrometer (IRIS)  
141 observations [63]. This is close to the protosolar He/ $\text{H}_2$  ratio of  $0.17$  [64] and may suggest  $\text{H}_2$   
142 and He gas were captured directly from the solar nebula. However, [63] show that nitrogen  
143 abundances from  $0$ – $0.006$  can also provide reasonable fits to the Voyager IRIS spectra, resulting  
144 in possible He/ $\text{H}_2$  ratios of  $0.08$ – $0.22$  by volume and leaving open the possibility that Neptune  
145 could have sub-solar or super-solar He/ $\text{H}_2$ . Nevertheless, the fact that Neptune's atmosphere  
146 is primarily composed of hydrogen and helium implies Neptune had to reach sufficient size  
147 for direct gravitational accretion fairly rapidly, because the lifetime of the protosolar nebula is  
148 estimated at  $\leq 10$  Myr [26,65]. Therefore, the hydrogen and helium abundance do not discriminate  
149 between ice and rock giant interior structures, but are important when considering hydrogen  
150 sources for interpretation of the D/H and O/H observations.

### 151 (ii) C/H from $\text{CH}_4$

152 On Neptune methane does not condense until  $\sim 1$ – $2$  bar, meaning that the abundance at higher  
153 pressures can be considered representative of Neptune's interior, assuming the interior is fully  
154 mixed. Neptune's tropospheric methane varies significantly with latitude, but has a globally-  
155 averaged volume mixing ratio of  $\sim 2$ – $5\%$  for pressures deeper than the condensation level [66–69].  
156 This large range of abundances shows that, even below the condensation level, condensible  
157 species can exhibit considerable variation due to atmospheric dynamics. Dynamics is also thought  
158 to cause the large variations in Jupiter's ammonia distribution recently observed at  $\sim 10$  bar  
159 by Juno [70,71]. These variations increase the uncertainty on Neptune's deep  $\text{CH}_4$  abundance  
160 and raise doubts about how representative the measured  $\text{CH}_4$  abundance really is of interior  
161 composition. Nevertheless,  $\text{CH}_4$  is the major carrier of carbon in Neptune's atmosphere and,  
162 if its abundance is representative of the interior, implies a C/H enrichment of  $50$ – $100$  times  
163 solar [64]. To date this remains the most reliable and direct indicator of elemental enrichment  
164 in Neptune [26], despite the large uncertainties.

### 165 (iii) D/H from $\text{H}_2$

166 The D/H ratio is also an important indicator of interior composition and formation [26,  
167 72]. Enrichment in Neptune's D/H ratio compared to solar composition is thought to be  
168 due to a significant fraction of enriched protoplanetary ices being mixed into Neptune's  
169 interior fluid envelope. D/H in Neptune's atmosphere is  $4.1 \pm 0.4 \times 10^{-5}$ , derived from Herschel  
170 observations of hydrogen [24]. This is around twice as enriched as the protosolar ratio of  
171  $(D/H)_{\text{proto}} = 2.25 \pm 0.35 \times 10^{-5}$  inferred from observations of Jupiter by ISO and Cassini [73,74].  
172 Present day ice reservoirs, including icy moons, comets, and Kuiper belt objects (KBOs), have  
173 variable D/H in the range  $(D/H)_{\text{ices}} = 15$ – $60 \times 10^{-5}$  [26,75–77]. Deriving an interior ice fraction  
174 from Neptune's D/H ratio is not straight forward and depends on many assumptions. Consider



175 a simple case where we assume: 1) present day ices have similar D/H ratios to neptunesimals  
 176 (planetesimals which formed Neptune); 2) Neptune has a rocky core overlain by an interior  
 177 fluid envelope and an outer gaseous fluid envelope; 3) the neptunesimals' rock component is  
 178 sequestered into the planetary core; and 4) the neptunesimals' ice component is well mixed and  
 179 thermodynamically equilibrated between Neptune's internal fluid and outer gaseous envelopes,  
 180 such that the measured D/H ratio is representative of the interior. In this case we can estimate the  
 181 proportion of ices in Neptune's combined fluid envelope following an approach similar to [72]:

$$\left(\frac{D}{H}\right)_{env} = x \left(\frac{D}{H}\right)_{proto} + (1-x) \left(\frac{D}{H}\right)_{ice} \quad (2.1)$$

where,  $x$  is the mole fraction of  $H_2$  accreted directly from the protosolar nebula,  $(1-x)$  is the mole fraction of  $H_2$  supplied by ices (in the form of water), and  $(D/H)_{env}$  is the observed atmospheric value. Under the above assumptions this implies  $x=0.85-0.97$ , i.e.,  $<15\%$  ice by mole fraction. This can be used to infer an envelope value for  $O/H = (1-x)/(2x + 2(1-x))$ , i.e. atoms of O from  $H_2O$  / atoms of H from  $H_2$  and  $H_2O$ . The overall relation between D/H and O/H in Neptune's fluid envelope under these simple assumptions is then:

$$\left(\frac{O}{H}\right)_{env} = \frac{1}{2} \left[ \left(\frac{D}{H}\right)_{env} - \left(\frac{D}{H}\right)_{proto} \right] / \left[ \left(\frac{D}{H}\right)_{ice} - \left(\frac{D}{H}\right)_{proto} \right] \quad (2.2)$$

182 corresponding to  $(O/H)_{env}=0.02-0.07$ . This implies an O/H enrichment in Neptune of 30–130  
 183 times the solar O/H value of  $5.4 \times 10^{-4}$  [64] in the fluid envelope (i.e., not including the core if  
 184 present). However, if there were incomplete mixing and equilibration in the interior, the deep  
 185 D/H ratio could be much greater than that in the observable atmosphere. In this case the  
 186 proportion of ice in the interior fluid envelope could be much larger.

187 One argument against incomplete mixing and equilibration is that Uranus' D/H ratio of  
 188  $4.4 \pm 0.4 \times 10^{-5}$  is very similar to Neptune's [24], despite very different internal heat fluxes [46,78]  
 189 and different internal structures [9,10]. Neptune has a bulk density of  $1.6 \text{ kg m}^{-3}$  and Uranus  
 190 is slightly less dense with a bulk density of  $1.3 \text{ kg m}^{-3}$  [9]. If both planets were formed from  
 191 similar ices, but in different amounts as indicated by their different densities, and had different  
 192 internal mixing/equilibration states, the similarity of their D/H ratios would be quite a strange  
 193 coincidence.

#### 194 (iv) O/H from CO, $H_2O$ and CS

195 Neptune's atmospheric carbon monoxide has implications for both external sources and internal  
 196 bulk composition. As a result, CO has received much observational attention, and has been  
 197 determined from sub-mm ground-based and space-based telescope observations by many studies  
 198 [25,39,42–44,79,80]. In sub-mm spectra, CO emission cores are sensitive to the stratospheric  
 199 abundance, whereas wide absorption wings are sensitive to tropospheric abundance, allowing  
 200 some details of the CO vertical profile to be determined. Nominal abundances of  $\sim 1$  ppm (parts  
 201 per million) CO in the stratosphere and  $\sim 0.1$  ppm in the troposphere are required to fit the  
 202 observed spectra. However, there is significant variation between the different studies (Figure 2)  
 203 and a consensus on tropospheric abundance has not yet been achieved.

204 The least controversial aspect of Neptune's CO profile is that there is a significant amount,  
 205  $\sim 1-2$  ppm, in the stratosphere at millibar pressures. The fact that the stratospheric abundance is  
 206 greater than the tropospheric abundance implies that Neptune's stratospheric CO must have an  
 207 external origin [79]. Neptune's stratospheric  $H_2O$  abundance of  $\sim 1.5-3.5$  ppb (parts per billion)  
 208 [81] must also have an external origin as water condenses deep in Neptune's interior at  $\sim 100-$   
 209  $1000$  bar, depending on the deep temperature profile. However, if both CO and  $H_2O$  are from  
 210 the same external source it is not possible to explain the three orders of magnitude abundance  
 211 difference with a steady state flux of ices, interplanetary dust, or micrometeorites [82]. The most  
 212 plausible way to explain the stratospheric CO- $H_2O$  discrepancy is if Neptune experienced a large

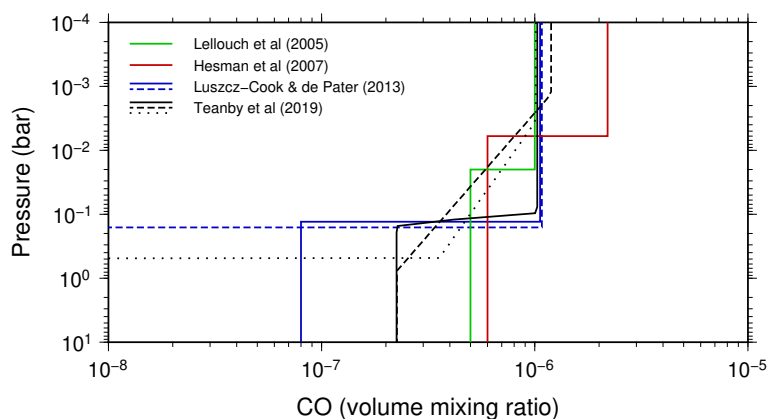


**Figure 2.** Neptune's CO profile. A comparison of recent studies shows a wide range of CO profiles can fit sub-mm spectra of Neptune. In the stratosphere at  $\sim 1$  mbar there is a broadly consistent 1–2 ppm abundance, but in the troposphere there are inconsistent results ranging from 0–0.5 ppm, indicating the deep CO profile is poorly constrained.

213 kilometre-scale comet impact in the last few hundred to a thousand years and that most of the  
 214 cometary  $H_2O$  was converted to CO by shock chemistry [79,82,83]. This is supported by recent  
 215 observations of CS in Neptune's upper stratosphere in trace amounts (20–200 parts per trillion)  
 216 [83]. CS is a shock chemistry product and was observed in Jupiter's stratosphere after the impact  
 217 of SL9 [84]. The stratospheric CO abundance is thus not relevant to understanding Neptune's  
 218 interior, but its presence does complicate the interpretation of atmospheric composition.

219 Neptune's tropospheric CO does have important implications for the internal composition  
 220 and O/H enrichment, but is sadly much more controversial. Some interpretations have deep  
 221 tropospheric CO as high as 0.5 ppm [44,79,80], whereas others are consistent with no CO in  
 222 the deep troposphere [25,44]. The issue is that tropospheric CO is derived from wide CO line-  
 223 wing absorption, which only provides moderate constraints on the CO profile and may not  
 224 provide information about pressures higher than  $\sim 1$  bar or so. This is because the line-wing  
 225 profile caused by tropospheric CO is degenerate with the uncertain tropospheric temperature  
 226 profile. Furthermore, many studies have required multiple observations to be stitched together  
 227 to give enough frequency range to cover the entire wing region (e.g., [44,79,80]), which can  
 228 introduce baseline shifts and cause additional uncertainties. The exact CO pressure sensitivity  
 229 also strongly depends on the uncertain temperature profile and assumptions about the form of the  
 230 CO profile itself, making the problem highly non-unique [25]. Given the under-constrained nature  
 231 of the problem, simple step-type functions are often used to fit the observations with only three  
 232 parameters: tropospheric abundance; stratospheric abundance; and transition pressure. These  
 233 profiles are surprisingly good at fitting the observations to within error, but are not likely to  
 234 be realistic representations of Neptune's CO profile and extreme caution must be used when  
 235 interpreting them - especially the deep abundance. However, at least some CO must be present in  
 236 the upper troposphere to explain the observed CO line-wing absorptions and there are currently  
 237 two hypotheses about the tropospheric CO profile.

The first and most widely adopted hypothesis is that significant CO exists throughout Neptune's troposphere, well mixed by vigorous convection from the deep interior up to the tropopause [44,79,85]. In thermochemical equilibrium, the mixing ratio of CO is controlled by the net reaction [86]:



238 In the cold upper troposphere, the right-hand-side of reaction (2.3) is strongly favoured, and  
 239 CO is not expected to be present in anywhere near observable abundances if thermochemical



equilibrium prevails. However, at high temperatures ( $>1000$  K) in the deep troposphere ( $>1000$  bar), the thermochemical equilibrium abundance of CO is many orders of magnitude larger. To explain  $\sim 0.1$  ppm levels of upper tropospheric CO from an interior source, the atmosphere cannot be in thermochemical equilibrium. Instead, models require a large interior O/H enrichment combined with rapid advection of deep-tropospheric gases, allowing the CO mixing ratio to be quenched at a deep-atmosphere abundance and reaction (2.3) to cease being effective because of the reduced reaction rate at lower temperatures [44,85–87]. For this to happen the mixing timescale must be much less than the loss timescale [44]. The required magnitude of O/H enrichment relative to solar composition depends on details of the chemical scheme, but ranges from 250–650 [44,85,86,88], with an O/H enrichment of  $\sim 250$  being inferred in the most recent study [88].

The second and more fringe hypothesis is that CO only exists in the upper troposphere, at pressures of a few bar or less [25]. In this case tropospheric CO is sourced from the same external comet as the stratospheric CO, not from the deep interior. This allows fitting of the sub-mm spectra without the need for extreme interior O/H enrichment. However, for this to be viable there cannot be vigorous mixing right up to the tropopause, or the upper tropospheric CO would be lost by mixing into the deep interior.

To illustrate the non-uniqueness of spectroscopic sensitivity to tropospheric CO we performed a synthetic retrieval test. We define an atmospheric model based on [25] with a CO profile that has no CO at pressures greater than 1 bar (Figure 3a), representative of an external source only profile [25]. The 1 bar pressure cut-off was chosen to be consistent with the approximate location of the radiative-convective boundary; it is plausible that the abundance of externally sourced CO could be relatively stable at lower pressures than this, but at higher pressures external CO would be lost to the deep interior via vigorous tropospheric mixing. A synthetic spectrum was then generated using the NEMESIS retrieval code [90] for the 115 GHz CO (1-0) line, which is the lowest frequency rotational CO line that probes the deepest in Neptune's atmosphere (Figure 3b). Random Gaussian noise was applied to this spectrum with a standard deviation of  $1/1000^{\text{th}}$  the continuum level (i.e., signal-to-noise = 1000), which is the dynamic range limit of ALMA, the highest sensitivity sub-mm observatory currently available. This observation then represents a best-case scenario for determining the deep CO profile. The CO profile was then inverted from the synthetic spectrum using three types of parameterised profiles: a simple step as commonly used in the literature; a step with a gradient instead of a sharp transition; and an external profile with an upper tropospheric gradient and zero deep abundance. Both gradient profiles could adequately fit the synthetic spectrum within errors, but the simple step slightly under-fits the line wings. However, if small perturbations to the temperature profiles within the 5 K uncertainty were allowed (Figure 3c) then the simple step could fully fit the synthetic spectrum to within errors (Figure 3d). Furthermore, if a slightly lower but still impressive signal-to-noise of 500 was obtained, the step function would be entirely consistent with the measurement without the need for any temperature profile adjustments. The same problem exists the other way around, i.e., an external gradient profile could fit a synthetic made with a step function to within errors. This illustrates the non-uniqueness of obtaining a CO profile on Neptune and explains why there are such a wide range of profiles in the literature. Even with ideal observations, an unrepresentative CO profile can give an excellent fit to the data and provide misleading information about deep CO abundance. The real atmosphere is likely to have some amount of disequilibrium CO being dredged up from the interior, but existing observations are unable to constrain this amount.

### 3. Interpretation of atmospheric observations

Implications from individual atmospheric observations are often inconsistent and difficult to fit into a single formation model [24,91,92]. Here we consider each of the ice and rock giant interior models and determine what is required to incorporate the atmospheric observations into a self-consistent theory. Figure 4 attempts to illustrate the implications of existing atmospheric

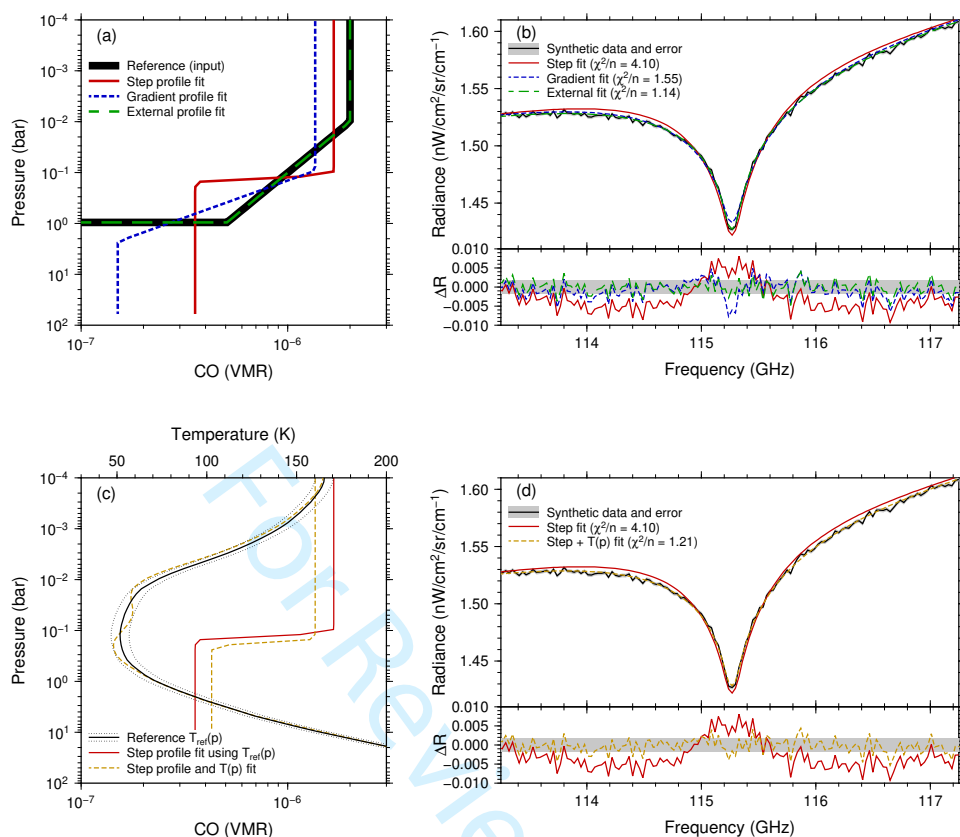


**Figure 3.** CO (1-0) line sensitivity test. (a) Reference profile used to generate the synthetic spectrum along with best fitting step and gradient profiles. (b) Fits to synthetic data using different profile parameterisations. All profiles provide a reasonable fit to the spectrum, although the step profile under-fits the line wings. (c) A slight adjustment to the temperature profile and step profile transition pressure can drastically improve the fit to the spectrum (d), even though the parameterisation is not representative of the true profile. This illustrates the non-uniqueness of the observations and the challenge of obtaining accurate CO profiles from remote sensing.  $\chi^2/n$  is the reduced chi-squared misfit and should be around unity for a fit consistent with measurement uncertainties [89].  $\Delta R$  is the difference between synthetic data and fitted spectra.

290 observations for Neptune's interior composition and how they could fit into ice- or rock-  
 291 dominated interior models. The interdependence of using atmospheric constraints, both on each  
 292 other and on uncertain assumptions, results in a rather complex and confusing picture. Both rock  
 293 and ice giants with various degrees of interior mixing can fit the observed fundamental physical  
 294 properties, which further adds to the uncertainty.

### 295 (a) Ice giant

296 The conventional model of Neptune (and Uranus) is an ice giant, where the interior comprises a  
 297 large fraction of ices (up to 90% by mass), mostly in the form of water ice. The ice giant model  
 298 has the advantage of having a large reservoir of interior water, that could act as a conductor for  
 299 driving the magnetic dynamo. The large fraction of ice is also compatible with extreme O/H  
 300 enrichment, providing an internal source for tropospheric CO.

301 However, there are significant problems with having a planet with this much ice. The main  
 302 issue is that if the interior is fully mixed and equilibrated, the inferred O/H enrichment from

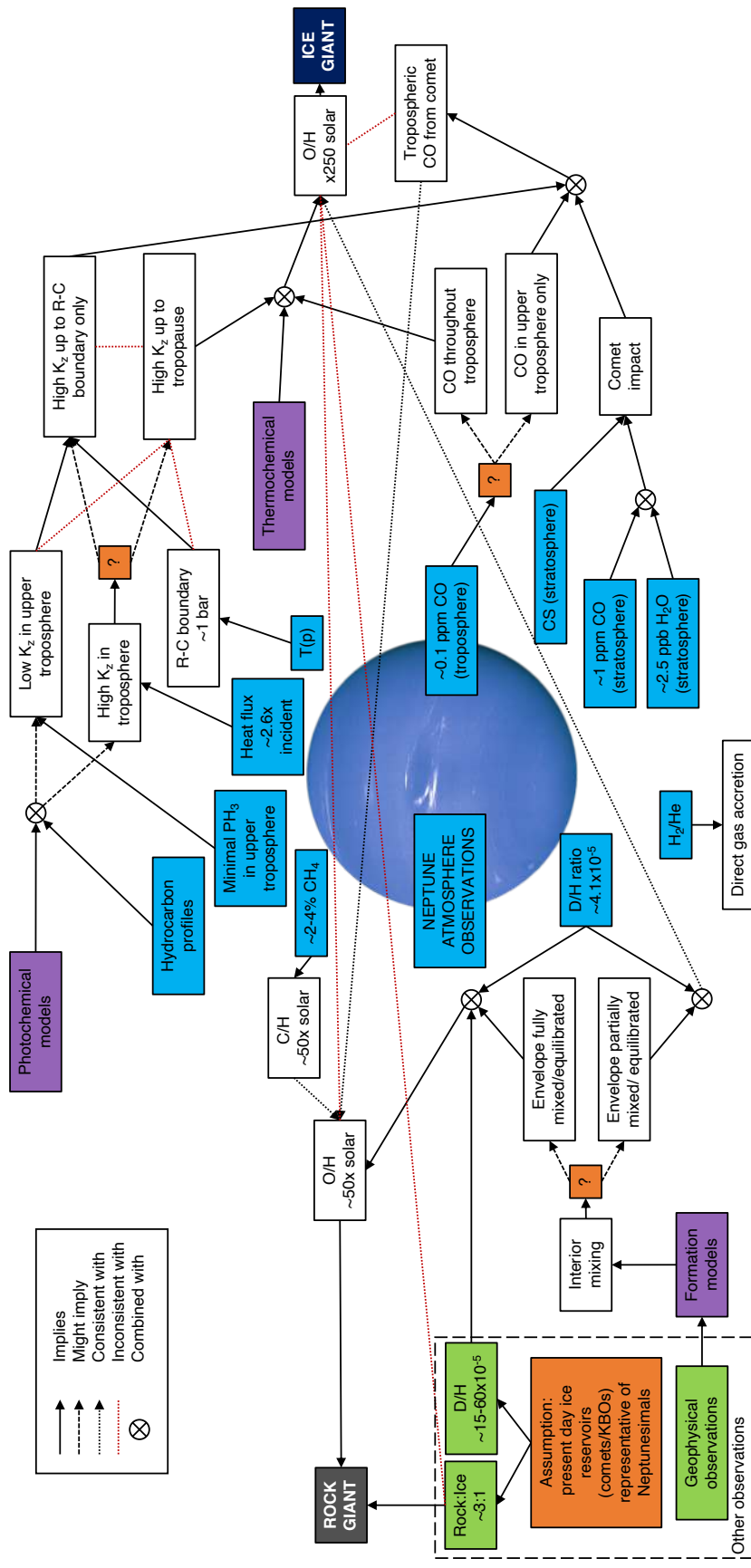


**Figure 4.** Schematic of Neptune's atmospheric constraints and uncertainties in their interpretation. Key unknowns are shown in orange and imply that it is not possible to definitively distinguish rock and ice giant interiors.

3003 D/H and CO observations are incompatible. O/H enrichment is inferred to be  $\sim 30$ – $130$  from the  
3004 observed D/H ratio, whereas O/H enrichment  $>250$  is inferred based on a deep tropospheric  
3005 CO mixing ratio of  $>0.1$  ppm. This must be reconciled somehow and there are currently three  
3006 potential explanations that could be invoked to solve this for the ice giant scenario.

3007 The first solution is if the neptunesimals were depleted in deuterium compared to present day  
3008 ices and that these exotic ices are no longer present in the solar system, with the justification being  
3009 that they were all used during planet formation. This seems highly unlikely as it relies on ices that  
3010 have not been observed anywhere in the solar system and would even be depleted in deuterium  
3011 compared to Earth's oceans.

3012 A second and more plausible solution is that the interior of Neptune is not completely mixed,  
3013 so that the measured atmospheric D/H ratio is not representative of the bulk planet. However,  
3014 the similarity of D/H ratios on Uranus and Neptune [24] is then very difficult to explain if the  
3015 planets experienced different degrees of mixing, as suggested by their different densities [5,6] and  
3016 very different heat fluxes [46,78], except by coincidence.

3017 A third alternative is if Neptune formed on the CO ice line. Initial modelling using a static  
3018 protosolar nebula and a simplified instantaneous condensation scheme suggested that outward  
3019 diffusion of CO vapour driven by a steep concentration gradient near the ice line, coupled with  
3020 inward migration of icy pebbles due to gas drag, could result in a high density of CO-rich  
3021 pebbles at the ice line [93]. If Neptune formed at the ice line then these CO-rich pebbles could  
3022 explain Neptune's large internal CO source without requiring excessive overall O/H enrichment  
3023 or H<sub>2</sub>O abundance [93]. However, the CO ice line location is very sensitive to rapidly evolving  
3024 disc conditions [94], with a general tendency to move inwards as the solar nebula cools [95], so  
3025 considering disc evolution timescales is essential [96]. Recent modelling of condensation rates  
3026 in the protosolar nebula also shows that production of solids near the ice line is less efficient  
3027 than previously thought [96], making it difficult to form Neptune at this location effectively.  
3028 Furthermore, it would be very difficult to form both Neptune and Uranus this way because the  
3029 ice line would have to migrate from one planet forming location to the other, but remain stable  
3030 for long enough to build planets in each location, making this scenario even less likely if Neptune  
3031 and Uranus have similar internal compositions. For Neptune to form on the CO ice line, timescales  
3032 for planet formation, subsequent planet migration, and ice line evolution must all be compatible,  
3033 which is difficult to achieve in current models [92,96].

### 3034 (b) Rock giant

3035 In the rock giant model of Neptune, there are still significant quantities of ice in the interior,  
3036 but most of the heavy elements are supplied by rock instead of ice. The rock giant model has  
3037 the advantage that Neptune can be formed from more conventional objects with similar rock-ice  
3038 ratios to Pluto, giant planet moons, and KBOs. KBOs appear to have a wide range of relative  
3039 ice compositions from almost pure rock to almost pure ice with smaller objects tending to have  
3040 lower densities suggesting they are more ice-rich [97]. For example a large object such as Pluto  
3041 has a relatively high rock:ice ratio of  $\sim 3:1$  [98]. Recent observations and modelling show that a  
3042 rock fraction of  $\sim 0.7$  can in fact fit many of these objects, with variations in porosity explaining  
3043 the density-size trend rather than variations in ice content [99]. If Neptune were formed from  
3044 such objects the interior would be rock-dominated and have a much lower O/H enrichment,  
3045 perhaps around 30–130 times solar. A lower O/H enrichment would also be more consistent  
3046 with the 50–100 C/H enrichment, assuming typical Neptune formation scenarios, except those  
3047 in which the heavy elements derive from clathrate hydrates (e.g., [100]). Another advantage of a  
3048 rock giant is that the reduced fractional content of ice means that the D/H ratio can be explained  
3049 with primordial ices with a similar D/H enrichment to present day solar system ices, even in the  
3050 case of complete internal mixing, which allows a greater range of realistic formation scenarios  
3051 [9]. Additionally, sequestering significant quantities of rocky material in the cores of Uranus and  
3052 Neptune during planet formation could potentially explain the deficit of refractory material in  
3053 the surface of the Sun compared to similar stars without planets [101].

354 However, a rock giant interpretation would be at odds with significant tropospheric CO  
355 reported by many studies. This could be resolved if CO from a major external source has been  
356 slowly transported down from high altitudes to the upper troposphere near the  $\sim 1$  bar region  
357 before being removed by faster convective mixing below that level, with the internal source itself  
358 remaining much smaller than 0.1 ppm. An accurate CO profile is essential to test this possibility.  
359 Another potential problem with a rock giant is how to create the magnetic field, which requires  
360 a conductive medium in the interior to support dynamo action. Possibilities include a shallow  
361 conductive water-rich layer, sourced from the ice component of the rock-ice neptunesimals, or a  
362 conductive silicate-hydrogen mixture of some kind.

### 363 (c) Summary of interior constraints

364 From the schematic in Figure 4 it is evident that there are four key unknowns, which are essential  
365 to fully interpret atmospheric observations in terms of Neptune's interior:

- 366 • The deep extent of CO beyond the upper troposphere, which determines the bulk O/H  
367 enrichment.
- 368 • The tropospheric eddy mixing profile, which determines how the CO profile is  
369 interpreted.
- 370 • The extent of internal mixing and equilibration within Neptune, which determines how  
371 representative atmospheric measurements are of the interior .
- 372 • The source material of neptunesimals, which would allow the D/H ratio to be used to  
373 infer bulk ice abundance.

374 The simplest interpretation based on current observations and models is that Neptune is a  
375 rock giant, i.e., Neptune formed with more rock than ice (Figure 4). However, under different  
376 assumptions both ice and rock giant interpretations are possible.

### 377 (d) Extension to Uranus

378 While this paper has focused on Neptune, similar arguments could also be made for Uranus. The  
379 D/H ratios are very similar on Uranus ( $D/H=4.4\pm 0.4\times 10^{-5}$ ) and Neptune ( $D/H=4.1\pm 0.4\times 10^{-5}$ )  
380 [24], suggesting a similar O/H enrichment if Uranus' interior is fully mixed. The tropospheric  
381 methane abundance on Uranus is also  $\sim 2\text{--}4\%$  [102,103], suggesting a similar C/H enrichment.  
382 Many hydrocarbons have also been observed in Uranus' atmosphere [104], but not CS. The  
383 main difference in observed atmospheric composition between Uranus and Neptune that has  
384 relevance to the interior structure is the measured CO abundance. Uranus' stratospheric CO is  
385  $\sim 8\pm 1$  ppb [105], which is much lower abundance than Neptune's  $\sim 1$  ppm. CO has not been  
386 detected at all in Uranus' troposphere, with a  $3\sigma$  upper limit of  $< 2.1$  ppb [31], again much lower  
387 than Neptune's  $\sim 0.1$  ppm. Therefore, the case for a rock giant is in fact simpler for Uranus as  
388 there is no requirement to dredge up CO from a strongly oxygen enriched interior to explain the  
389 tropospheric composition. The lack of tropospheric CO could then be explained by either: lack of  
390 a large cometary impact in the rock giant case; or by reduced tropospheric convection in the ice  
391 giant case, as inferred from the low emitted infrared flux [78]. The D/H ratio is again the strongest  
392 argument in favour of the rock giant scenario, although as for Neptune, for this to have relevance  
393 to the interior requires a well mixed fluid envelope [9,24].

## 394 4. Conclusion

395 Current observational constraints from fundamental physical properties are consistent with both  
396 ice and rock giant interpretations of Neptune's internal structure. Further constraints are available  
397 from observations of the atmosphere, which we consider in this paper, but it is difficult to  
398 definitively interpret these measurements in terms of the planetary bulk composition because



399 interpretation strongly depends on model assumptions or physical and chemical processes that  
400 are not fully understood. In addition, measured abundances are likely influenced by “pollution”  
401 from recent comet impact(s), which makes the problem even more challenging. Therefore,  
402 observations of Neptune’s atmosphere are somewhat ambiguous and can support either model,  
403 depending on what is assumed during the interpretation.

404 Abundant tropospheric CO has previously been used to argue a preference for the ice giant  
405 interpretation, with extreme internal O/H enrichments of  $>250$ , but on closer inspection the  
406 evidence for CO at pressures above a few bar is not convincing. Such a model would also most  
407 likely require incomplete interior mixing during formation to explain Neptune’s low atmospheric  
408 D/H ratio.

409 Cometary CO and reduced upper tropospheric mixing provides an alternative explanation  
410 for Neptune’s CO profile, and is consistent with arguments based on the observed lapse rate  
411 and photochemical model comparisons. This could favour a rock giant interpretation, formed  
412 from rock-ice mixtures with similar properties to present day solar system objects, resulting in  
413 O/H enrichments similar to C/H. This has the advantage of reconciling Neptune’s CO and D/H  
414 measurements and using known ice sources.

415 A similar case can also be made for Uranus being a rock giant. The case for Uranus is in fact  
416 more straight forward, as there is no observed tropospheric CO requiring an explanation, either  
417 in terms of highly enriched O/H or external cometary source.

418 Definitively distinguishing between ice and rock giant scenarios on Uranus and Neptune  
419 will require a dedicated future mission with orbiter and entry probe elements [28,29,106]. A  
420 key measurement to make with such a probe would be the CO profile down to at least 10 bar  
421 from a mass spectrometer. However, both CO and N<sub>2</sub> have a molecular mass of 28, making  
422 this a difficult observation. N<sub>2</sub> is also predicted to be an important disequilibrium quenched  
423 constituent being dredged up from the deep atmosphere, so any instrumentation on an *in situ*  
424 Neptune/Uranus probe would need some way of distinguishing CO from N<sub>2</sub> [26,30], which was  
425 not possible with the mass spectrometer included on the Galileo probe to Jupiter [107]. If such a  
426 CO measurement were possible, it would provide a more definitive measure of Neptune’s O/H  
427 enrichment. Such a measurement is not possible from Earth as even the deepest sounding CO 1-0  
428 line can be interpreted in multiple ways and may only be sensitive to a few bar, which is not far  
429 enough into the well mixed region to be representative. Measurements of the noble gases are also  
430 essential for constraining formation scenarios, but are currently unconstrained as they require  
431 in-situ measurement. Neon is soluble in liquid helium so may be depleted, but argon, krypton,  
432 and xenon are not so can be used to determine neptunesimal composition, in particular they can  
433 distinguish between icy planetestimals, clathrates, and ice line formation scenarios [26].

434 It would be essential to complement any probe measurements with orbital mapping to provide  
435 global context. Observations of Jupiter with Juno show that internally sourced species can be  
436 highly variable to high pressures of  $\sim 10$  bar or more [70,71], suggesting the troposphere on  
437 Neptune/Uranus may not be well mixed compositionally [106]. Orbital mapping of deep CO  
438 at Neptune would be challenging and require a very high specification sub-mm sounder that was  
439 carefully designed to be sensitive to deep abundance. Orbital measurements would also vastly  
440 improve constraints on fundamental physical properties, particularly high order gravitational  
441 coefficients, which can be used to constrain internal structure [9,70,108], and the magnetic field  
442 structure and origin.

443 Uranus and Neptune’s interiors remain a mystery that urgently requires a new mission to  
444 solve. This will not only reveal the formation and evolution of these enigmatic worlds, but will  
445 also unlock new insights into our solar system’s evolution.

446 **Authors’ Contributions.** NAT conceived the study and wrote the initial manuscript. All authors read and  
447 contributed to the final manuscript.

448 **Competing Interests.** The authors declare that they have no competing interests.

449 **Funding.** NAT and PGJI were funded by the UK Science and Technology Facilities Council (STFC). JIM  
450 acknowledges support from the NASA Solar System Workings grant 80NSSC19K0536. RH acknowledges  
451 support from the Swiss National Science Foundation (SNSF) via grant 200020\_188460.

452 **Acknowledgements.** The authors are grateful to Mark Hofstadter, Tristan Guillot, and an anonymous  
 453 reviewer for their insightful comments, which helped improve the manuscript.

## 454 References

- 455 1. Tyler GL, Sweetnam DN, Anderson JD, Campbell JK, Eshleman VR, Hinson DP, Levy GS,  
 456 Lindal GF, Marouf EA, Simpson RA. 1986 Voyager 2 radio science observations of the Uranian  
 457 system: atmosphere, rings, and satellites. *Science* **233**, 79–84.
- 458 2. Tyler GL, Sweetnam DN, Anderson JD, Borutzki SE, Campbell JK, Eshleman VR, Gresh DL,  
 459 Gurrola EM, Hinson DP, Kawashima N, Kursinski ER, Levy GS, Lindal GF, Lyons JR, Marouf  
 460 EA, Rosen PA, Simpson RA, Wood GE. 1989 Voyager radio science observations of Neptune  
 461 and Triton. *Science* **246**, 1466–1473.
- 462 3. Jacobson RA. 2009 The orbits of the Neptunian satellites and the orientation of the pole of  
 463 Neptune. *Astron. J.* **137**, 4322–4329.
- 464 4. Jacobson RA. 2014 The Orbits of the Uranian satellites and rings, the gravity field of the  
 465 Uranian system, and the orientation of the pole of Uranus. *Astron. J.* **148**, 76.
- 466 5. Podolak M, Hubbard W, Stevenson DJ. 1991 Models of Uranus' interior and magnetic field.  
 467 In Bergstralh J, Miner E, Shapley Matthews M, editors, *Uranus* Space Science Series pp. 29–61  
 468 Tucson. University of Arizona Press.
- 469 6. Hubbard WB, Podolak M, Stevenson DJ. 1995 The interior of Neptune. In Cruikshank DP,  
 470 Matthews MS, Schumann AM, editors, *Neptune and Triton* Space Science Series pp. 109–138  
 471 Tucson. University of Arizona Press.
- 472 7. Hubbard WB, Nellis WJ, Mitchell AC, Holmes NC, Limaye SS, McCandless PC. 1991 Interior  
 473 structure of Neptune: comparison with Uranus. *Science* **253**, 648–651.
- 474 8. Podolak M, Weizman A, Marley M. 1995 Comparative models of Uranus and Neptune. *Plan.*  
 475 *& Space Sci.* **43**, 1517–1522.
- 476 9. Helled R, Nettelmann N, Guillot T. 2020 Uranus and Neptune: origin, evolution and internal  
 477 structure. *Space Sci. Rev.* **216**, 38.
- 478 10. Helled R, Fortney J. 2020 The interior structure of Uranus and Neptune: current  
 479 understanding and open questions. *Phil. Trans. R. Soc. Lond. A* **current issue, under review**.
- 480 11. Ness NF, Acuna MH, Behannon KW, Burlaga LF, Connerney JEP, Lepping RP, Neubauer FM.  
 481 1986 Magnetic fields at Uranus. *Science* **233**, 85–89.
- 482 12. Connerney JEP, Acuna MH, Ness NF. 1987 The magnetic field of Uranus. *J. Geophys. Res.* **92**,  
 483 15329–15336.
- 484 13. Connerney JEP, Acuna MH, Ness NF. 1991 The magnetic field of Neptune. *J. Geophys. Res.* **96**,  
 485 19023–19042.
- 486 14. Ness N, Acuña M, Connerney J. 1995 Neptune's magnetic field and field-geometric properties.  
 487 In Cruikshank DP, Matthews MS, Schumann AM, editors, *Neptune and Triton* Space Science  
 488 Series pp. 141–168 Tucson. University of Arizona Press.
- 489 15. Stanley S, Bloxham J. 2004 Convective-region geometry as the cause of Uranus' and Neptune's  
 490 unusual magnetic fields. *Nature* **428**, 151–153.
- 491 16. Soderlund K. 2020 Ice giant dynamos. *Phil. Trans. R. Soc. Lond. A* **current issue, under review**.
- 492 17. Millot M, Hamel S, Rygg JR, Celliers PM, Collins GW, Coppari F, Fratanduono DE, Jeanloz  
 493 R, Swift DC, Eggert JH. 2018 Experimental evidence for superionic water ice using shock  
 494 compression. *Nature Physics* **14**, 297–302.
- 495 18. Soubiran F, Militzer B. 2018 Electrical conductivity and magnetic dynamos in magma oceans  
 496 of Super-Earths. *Nature Communications* **9**, 3883.
- 497 19. Millot M, Dubrovinskaia N, Černok A, Blaha S, Dubrovinsky L, Braun DG, Celliers PM,  
 498 Collins GW, Eggert JH, Jeanloz R. 2015 Shock compression of stishovite and melting of silica  
 499 at planetary interior conditions. *Science* **347**, 418–420.
- 500 20. Helled R, Stevenson D. 2017 The fuzziness of giant planets' cores. *Astrophys. J. Lett.* **840**, L4.
- 501 21. Fortney JJ, Nettelmann N. 2010 The interior structure, composition, and evolution of giant  
 502 planets. *Space Sci. Rev.* **152**, 423–447.
- 503 22. Helled R, Anderson JD, Podolak M, Schubert G. 2011 Interior models of Uranus and Neptune.  
 504 *Astrophys. J.* **726**, 15.
- 505 23. Nettelmann N, Helled R, Fortney JJ, Redmer R. 2013 New indication for a dichotomy in the  
 506 interior structure of Uranus and Neptune from the application of modified shape and rotation  
 507 data. *Plan. & Space Sci.* **77**, 143–151.

- 508 24. Feuchtgruber H, Lellouch E, Orton G, de Graauw T, Vandenbussche B, Swinyard B, Moreno R,  
509 Jarchow C, Billebaud F, Cavalié T, Sidher S, Hartogh P. 2013 The D/H ratio in the atmospheres  
510 of Uranus and Neptune from Herschel-PACS observations. *Astron. Astrophys.* **551**, 1–9.
- 511 25. Teanby NA, Irwin PGJ, Moses JI. 2019 Neptune’s carbon monoxide profile and phosphine  
512 upper limits from Herschel/SPIRE: implications for interior structure and formation. *Icarus*  
513 **319**, 86–98.
- 514 26. Atreya SK, Hofstadter MH, In JH, Mousis O, Reh K, Wong MH. 2020 Deep atmosphere  
515 composition, structure, origin, and exploration, with particular focus on critical in situ science  
516 at the icy giants. *Space Sci. Rev.* **216**, 18.
- 517 27. Arridge CS, Agnor CB, André N, Baines KH, Fletcher LN, Gautier D, Hofstadter MD, Jones  
518 GH, Lamy L, Langevin Y, Mousis O, Nettelmann N, Russell CT, Stallard T, Tiscareno MS, Tobie  
519 G, Bacon A, Chaloner C, Guest M, Kemble S, Peacocke L, Achilleos N, Andert TP, Banfield  
520 D, Barabash S, Barthelemy M, Bertucci C, Brandt P, Ceconi B, Chakrabarti S, Cheng AF,  
521 Christensen U, Christou A, Coates AJ, Collinson G, Cooper JF, Courtin R, Dougherty MK,  
522 Ebert RW, Entradas M, Fazakerley AN, Fortney JJ, Galand M, Gustin J, Hedman M, Helled  
523 R, Henri P, Hess S, Holme R, Karatekin Ö, Krupp N, Leisner J, Martin-Torres J, Masters A,  
524 Melin H, Miller S, Müller-Wodarg I, Noyelles B, Paranicas C, de Pater I, Pätzold M, Prangé  
525 R, Quémerais E, Roussos E, Rymer AM, Sánchez-Lavega A, Saur J, Sayanagi KM, Schenk P,  
526 Schubert G, Sergis N, Sohl F, Sittler EC, Teanby NA, Tellmann S, Turtle EP, Vinatier S, Wahlund  
527 JE, Zarka P. 2012 Uranus Pathfinder: exploring the origins and evolution of ice giant planets.  
528 *Experimental Astronomy* **33**, 753–791.
- 529 28. Hofstadter M, Simon A, Atreya S, Banfield D, Fortney JJ, Hayes A, Hedman M, Hospodarsky  
530 G, Mandt K, Masters A, Showalter M, Soderlund KM, Turrini D, Turtle E, Reh K, Elliott J,  
531 Arora N, Petropoulos A, Ice Giant Mission Study Team. 2019 Uranus and Neptune missions:  
532 a study in advance of the next Planetary Science Decadal Survey. *Plan. & Space Sci.* **177**, 104680.
- 533 29. Mousis O, Atkinson DH, Ambrosi R, Atreya S, Banfield D, Barabash S, Blanc M, Cavalié T,  
534 Coustenis A, Deleuil M, Durré G, Ferri F, Fletcher L, Fouchet T, Guillot T, Hartogh P, Hueso  
535 R, Hofstadter M, Lebreton JP, Mandt KE, Rauer H, Rannou P, Renard JB, Sanchez-Lávega A,  
536 Sayanagi K, Simon A, Spilker T, Venkatapathy E, Waite JH, Wurz P. 2019 In situ exploration of  
537 the giant planets. *arXiv e-prints* p. arXiv:1908.00917.
- 538 30. Cavalié T, Venot O, Miguel Y, Fletcher LN, Wurz P, Mousis O, Bounaceur R, Hue V, Leconte  
539 J, Dobrijevic M. 2020 The deep composition of Uranus and Neptune from in situ exploration  
540 and thermochemical modeling. *Space Sci. Rev.* **216**, 58.
- 541 31. Teanby NA, Irwin PGJ. 2013 An external origin for carbon monoxide on Uranus from  
542 Herschel/SPIRE?. *Astrophys. J. Lett.* **775**, L49.
- 543 32. de Pater I, Massie ST. 1985 Models of the millimeter-centimeter spectra of the giant planets.  
544 *Icarus* **62**, 143–171.
- 545 33. Hofstadter MD, Butler BJ. 2003 Seasonal change in the deep atmosphere of Uranus. *Icarus* **165**,  
546 168–180.
- 547 34. Janssen MA, Oswald JE, Brown ST, Gulkis S, Levin SM, Bolton SJ, Allison MD, Atreya SK,  
548 Gautier D, Ingersoll AP, Lunine JI, Orton GS, Owen TC, Steffes PG, Adumitroaie V, Bellotti  
549 A, Jewell LA, Li C, Li L, Misra S, Oyafuso FA, Santos-Costa D, Sarkissian E, Williamson R,  
550 Arballo JK, Kitiyakara A, Ulloa-Severino A, Chen JC, Maiwald FW, Sahakian AS, Pingree  
551 PJ, Lee KA, Mazer AS, Redick R, Hodges RE, Hughes RC, Bedrosian G, Dawson DE,  
552 Hatch WA, Russell DS, Chamberlain NF, Zawadski MS, Khayatian B, Franklin BR, Conley  
553 HA, Kempenaar JG, Loo MS, Sunada ET, Vorperion V, Wang CC. 2017 MWR: Microwave  
554 Radiometer for the Juno Mission to Jupiter. *Space Sci. Rev.* **213**, 139–185.
- 555 35. de Pater I, Mitchell DL. 1993 Radio observations of the planets: the importance of laboratory  
556 measurements. *J. Geophys. Res.* **98**, 5471–5490.
- 557 36. de Pater I, Richmond M. 1989 Neptune’s microwave spectrum from 1 mm to 20 cm. *Icarus* **80**,  
558 1–13.
- 559 37. Irwin PGJ. 2009 *Giant planets of our solar system: atmospheres, composition, and structure*.  
560 Chichester UK: Springer-Praxis 2nd edition.
- 561 38. Lindal GF. 1992 The atmosphere of Neptune - an analysis of radio occultation data acquired  
562 with Voyager 2. *Astron. J.* **103**, 967–982.
- 563 39. Fletcher LN, Drossart P, Burgdorf M, Orton GS, Encrenaz T. 2010 Neptune’s atmospheric  
564 composition from AKARI infrared spectroscopy. *Astron. Astrophys.* **514**, A17.
- 565 40. Lindal GF, Lyons JR, Sweetnam DN, Eshleman VR, Hinson DP, Tyler GL. 1990 The atmosphere

- of Neptune: results of radio occultation measurements with the Voyager 2 spacecraft. *Geophys. Res. Lett.* **17**, 1733–1736.
41. Burgdorf M, Orton GS, Davis GR, Sidher SD, Feuchtgruber H, Griffin MJ, Swinyard BM. 2003 Neptune's far-infrared spectrum from the ISO long-wavelength and short-wavelength spectrometers. *Icarus* **164**, 244–253.
42. Marten A, Matthews HE, Owen T, Moreno R, Hidayat T, Biraud Y. 2005 Improved constraints on Neptune's atmosphere from submillimetre-wavelength observations. *Astron. Astrophys.* **429**, 1097–1105.
43. Lellouch E, Hartogh P, Feuchtgruber H, Vandenbussche B, de Graauw T, Moreno R, Jarchow C, Cavalié T, Orton G, Banaszkiwicz M, Blecka MI, Bockelée-Morvan D, Crovisier J, Encrenaz T, Fulton T, Küppers M, Lara LM, Lis DC, Medvedev AS, Rengel M, Sagawa H, Swinyard B, Szutowicz S, Bensch F, Bergin E, Billebaud F, Biver N, Blake GA, Blommaert JADL, Cernicharo J, Courtin R, Davis GR, Decin L, Encrenaz P, Gonzalez A, Jehin E, Kidger M, Naylor D, Portyankina G, Schieder R, Sidher S, Thomas N, de Val-Borro M, Verdugo E, Waelkens C, Walker H, Aarts H, Comito C, Kawamura JH, Maestrini A, Peacocke T, Teipen R, Tils T, Wildeman K. 2010 First results of Herschel-PACS observations of Neptune. *Astron. Astrophys.* **518**, L152.
44. Luszcz-Cook SH, de Pater I. 2013 Constraining the origins of Neptune's carbon monoxide abundance with CARMA millimeter-wave observations. *Icarus* **222**, 379–400.
45. Fletcher LN, Kaspi Y, Guillot T, Showman AP. 2020 How well do we understand the belt/zone circulation of giant planet atmospheres?. *Space Sci. Rev.* **216**, 30.
46. Fiering JC, Conrath BJ. 1991 The albedo, effective temperature, and energy balance of Neptune, as determined from Voyager data. *J. Geophys. Res.* **96**, 18921–18930.
47. Moses JI, Allen M, Yung YL. 1992 Hydrocarbon nucleation and aerosol formation in Neptune's atmosphere. *Icarus* **99**, 318–346.
48. Guillot T. 1995 Condensation of methane, ammonia, and water and the inhibition of convection in giant planets. *Science* **269**, 1697–1699.
49. Leconte J, Selsis F, Hersant F, Guillot T. 2017 Condensation-inhibited convection in hydrogen-rich atmospheres. Stability against double-diffusive processes and thermal profiles for Jupiter, Saturn, Uranus, and Neptune. *Astron. Astrophys.* **598**, A98.
50. Friedson AJ, Gonzales EJ. 2017 Inhibition of ordinary and diffusive convection in the water condensation zone of the ice giants and implications for their thermal evolution. *Icarus* **297**, 160–178.
51. Yelle RV, Herbert F, Sandel BR, Vervack, Ronald J. J, Wentzel TM. 1993 The distribution hydrocarbons in Neptune's upper atmosphere. *Icarus* **104**, 38–59.
52. Bishop J, Romani PN, Atreya SK. 1998 Voyager 2 ultraviolet spectrometer solar occultations at Neptune: photochemical modeling of the 125–165 nm lightcurves. *Plan. & Space Sci.* **46**, 1–20.
53. Parkinson CD, McConnell JC, Sand el BR, Yelle RV, Broadfoot AL. 1990 He 584 Å dayglow at Neptune. *Geophys. Res. Lett.* **17**, 1709–1712.
54. Bézard B, Romani PN, Conrath BJ, Maguire WC. 1991 Hydrocarbons in Neptune's stratosphere from Voyager infrared observations. *J. Geophys. Res.* **96**, 18961–18975.
55. Bishop J, Atreya SK, Romani PN, Sand el BR, Herbert F. 1992 Voyager 2 ultraviolet spectrometer solar occultations at Neptune: constraints on the abundance of methane in the stratosphere. *J. Geophys. Res.* **97**, 11681–11694.
56. Romani PN, Bishop J, Bézard B, Atreya S. 1993 Methane photochemistry on Neptune: ethane and acetylene mixing ratios and haze production. *Icarus* **106**, 442–463.
57. Moses JI, Fletcher LN, Greathouse TK, Orton GS, Hue V. 2018 Seasonal stratospheric photochemistry on Uranus and Neptune. *Icarus* **307**, 124–145.
58. Moses J, Cavalié T, Fletcher LN, Roman M. 2020 Atmospheric chemistry on Uranus and Neptune. *Phil. Trans. R. Soc. Lond. A* **current issue, under review**.
59. Moses JI. 1992 Meteoroid ablation in Neptune's atmosphere. *Icarus* **99**, 368–383.
60. Dobrijevic M, Loison JC, Hue V, Cavalié T, Hickson KM. 2020 1D photochemical model of the ionosphere and the stratosphere of Neptune. *Icarus* **335**, 113375.
61. Gautier D, Conrath B, Owen T, de Pater I, Atreya S. 1995 The troposphere of Neptune. In Cruikshank DP, Matthews MS, Schumann AM, editors, *Neptune and Triton* Space Science Series pp. 563–628 Tucson. University of Arizona Press.
62. Conrath BJ, Gautier D, Lindal GF, Samuelson RE, Shaffer WA. 1991 The helium abundance of Neptune from Voyager measurements. *J. Geophys. Res.* **96**, 18907–18919.



- 624 63. Conrath BJ, Gautier D, Owen TC, Samuelson RE. 1993 Constraints on N<sub>2</sub> in Neptune's  
625 atmosphere from Voyager measurements. *Icarus* **101**, 168–171.
- 626 64. Lodders K. 2010 Solar System abundances of the elements. In Goswami A, Reddy BE, editors,  
627 *Principles and Perspectives in Cosmochemistry* pp. 379–417 Berlin, Heidelberg. Springer Berlin  
628 Heidelberg.
- 629 65. Podosek FA, Cassen P. 1994 Theoretical, observational and isotopic estimates of the lifetime of  
630 the solar nebula. *Meteoritics* **29**, 6–25.
- 631 66. Baines KH, Mickelson ME, Larson LE, Ferguson DW. 1995 The abundances of methane  
632 and ortho/para hydrogen on Uranus and Neptune: implications of new laboratory 4-0 H<sub>2</sub>  
633 quadrupole line parameters. *Icarus* **114**, 328–340.
- 634 67. Karkoschka E, Tomasko MG. 2011 The haze and methane distributions on Neptune from HST-  
635 STIS spectroscopy. *Icarus* **211**, 780–797.
- 636 68. Tollefson J, de Pater I, Luszcz-Cook S, DeBoer D. 2019 Neptune's latitudinal variations as  
637 viewed with ALMA. *Astron. J.* **157**, 251.
- 638 69. Irwin PGJ, Toledo D, Braude AS, Bacon R, Weilbacher PM, Teanby NA, Fletcher LN, Orton GS.  
639 2019 Latitudinal variation in the abundance of methane (CH<sub>4</sub>) above the clouds in Neptune's  
640 atmosphere from VLT/MUSE narrow field mode observations. *Icarus* **331**, 69–82.
- 641 70. Bolton SJ, Adriani A, Adumitroaie V, Allison M, Anderson J, Atreya S, Bloxham J, Brown S,  
642 Connerney JEP, DeJong E, Folkner W, Gautier D, Grassi D, Gulkis S, Guillot T, Hansen C,  
643 Hubbard WB, Iess L, Ingersoll A, Janssen M, Jorgensen J, Kaspi Y, Levin SM, Li C, Lunine  
644 J, Miguel Y, Mura A, Orton G, Owen T, Ravine M, Smith E, Steffes P, Stone E, Stevenson D,  
645 Thorne R, Waite J, Durante D, Ebert RW, Greathouse TK, Hue V, Parisi M, Szalay JR, Wilson  
646 R. 2017 Jupiter's interior and deep atmosphere: the initial pole-to-pole passes with the Juno  
647 spacecraft. *Science* **356**, 821–825.
- 648 71. Li C, Ingersoll A, Janssen M, Levin S, Bolton S, Adumitroaie V, Allison M, Arballo J, Bellotti  
649 A, Brown S, Ewald S, Jewell L, Misra S, Orton G, Oyafuso F, Steffes P, Williamson R. 2017  
650 The distribution of ammonia on Jupiter from a preliminary inversion of Juno microwave  
651 radiometer data. *Geophys. Res. Lett.* **44**, 5317–5325.
- 652 72. Lecluse C, Robert F, Gautier D, Guiraud M. 1996 Deuterium enrichment in giant planets. *Plan.  
653 & Space Sci.* **44**, 1579–1592.
- 654 73. Lellouch E, Bézard B, Fouchet T, Feuchtgruber H, Encrenaz T, de Graauw T. 2001 The  
655 deuterium abundance in Jupiter and Saturn from ISO-SWS observations. *Astron. Astrophys.*  
656 **370**, 610–622.
- 657 74. Pierel JDR, Nixon CA, Lellouch E, Fletcher LN, Bjoraker GL, Achterberg RK, Bézard B,  
658 Hesman BE, Irwin PGJ, Flasar FM. 2017 D/H ratios on Saturn and Jupiter from Cassini CIRS.  
659 *Astron. J.* **154**, 178.
- 660 75. Hartogh P, Lis DC, Bockelée-Morvan D, de Val-Borro M, Biver N, Küppers M, Emprechtinger  
661 M, Bergin EA, Crovisier J, Rengel M, Moreno R, Szutowicz S, Blake GA. 2011 Ocean-like water  
662 in the Jupiter-family comet 103P/Hartley 2. *Nature* **478**, 218–220.
- 663 76. Bockelée-Morvan D, Biver N, Swinyard B, de Val-Borro M, Crovisier J, Hartogh P, Lis DC,  
664 Moreno R, Szutowicz S, Lellouch E, Emprechtinger M, Blake GA, Courtin R, Jarchow C,  
665 Kidger M, Küppers M, Rengel M, Davis GR, Fulton T, Naylor D, Sidher S, Walker H. 2012  
666 Herschel measurements of the D/H and <sup>16</sup>O/<sup>18</sup>O ratios in water in the Oort-cloud comet  
667 C/2009 P1 (Garradd). *Astron. Astrophys.* **544**, L15.
- 668 77. Altwegg K, Balsiger H, Bar-Nun A, Berthelier JJ, Bieler A, Bochsler P, Briois C, Calmonte U,  
669 Combi M, De Keyser J, Eberhardt P, Fiethe B, Fuselier S, Gasc S, Gombosi TI, Hansen KC,  
670 Hässig M, Jäckel A, Kopp E, Korth A, LeRoy L, Mall U, Marty B, Mousis O, Neefs E, Owen T,  
671 Rème H, Rubin M, Sémon T, Tzou CY, Waite H, Wurz P. 2015 67P/Churyumov-Gerasimenko,  
672 a Jupiter family comet with a high D/H ratio. *Science* **347**, 1261952.
- 673 78. Pearl JC, Conrath BJ, Hanel RA, Pirraglia JA, Coustenis A. 1990 The albedo, effective  
674 temperature, and energy balance of Uranus, as determined from Voyager IRIS data. *Icarus*  
675 **84**, 12–28.
- 676 79. Lellouch E, Moreno R, Paubert G. 2005 A dual origin for Neptune's carbon monoxide?. *Astron.  
677 Astrophys.* **430**, L37–L40.
- 678 80. Hesman BE, Davis GR, Matthews HE, Orton GS. 2007 The abundance profile of CO in  
679 Neptune's atmosphere. *Icarus* **186**, 342–353.
- 680 81. Feuchtgruber H, Lellouch E, de Graauw T, Bézard B, Encrenaz T, Griffin M. 1997 External  
681 supply of oxygen to the atmospheres of the giant planets. *Nature* **389**, 159–162.



- 682 82. Moses JI, Poppe AR. 2017 Dust ablation on the giant planets: consequences for stratospheric  
683 photochemistry. *Icarus* **297**, 33–58.
- 684 83. Moreno R, Lellouch E, Cavalié T, Moullet A. 2017 Detection of CS in Neptune’s atmosphere  
685 from ALMA observations. *Astron. Astrophys.* **608**, L5.
- 686 84. Lellouch E. 1996 Chemistry induced by the impacts: observations. In Noll KS, Weaver HA,  
687 Feldman PD, editors, *IAU Colloq. 156: The Collision of Comet Shoemaker-Levy 9 and Jupiter* pp.  
688 213–241.
- 689 85. Cavalié T, Venot O, Selsis F, Hersant F, Hartogh P, Leconte J. 2017 Thermochemistry and  
690 vertical mixing in the tropospheres of Uranus and Neptune: how convection inhibition can  
691 affect the derivation of deep oxygen abundances. *Icarus* **291**, 1–16.
- 692 86. Lodders K, Fegley, Jr. B. 1994 The origin of carbon monoxide in Neptunes’s atmosphere. *Icarus*  
693 **112**, 368–375.
- 694 87. Prinn RG, Barshay SS. 1977 Carbon monoxide on Jupiter and implications for atmospheric  
695 convection. *Science* **198**, 1031–1034.
- 696 88. Venot O, Cavalié T, Bounaceur R, Tremblin P, Brouillard L, Lhoussaine Ben Brahim R. 2020  
697 New chemical scheme for giant planet thermochemistry. Update of the methanol chemistry  
698 and new reduced chemical scheme. *Astron. Astrophys.* **634**, A78.
- 699 89. Press WH, Flannery BP, Teukolsky SA, Vetterling WT. 1992 *Numerical Recipes*. Cambridge UK:  
700 Cambridge Univ. Press 2<sup>nd</sup> edition.
- 701 90. Irwin P, Teanby N, de Kok R, Fletcher L, Howett C, Tsang C, Wilson C, Calcutt S, Nixon C,  
702 Parrish P. 2008 The NEMESIS planetary atmosphere radiative transfer and retrieval tool. *J.*  
703 *Quant. Spectro. Rad. Trans.* **109**, 1136–1150.
- 704 91. Ali-Dib M. 2017 A pebbles accretion model with chemistry and implications for the Solar  
705 system. *Mon. Not. R. Astron. Soc.* **464**, 4282–4298.
- 706 92. Mousis O, Aguichine A, Atkinson DH, Atreya SK, Cavalié T, Lunine JI, Mand t KE, Ronnet T.  
707 2020 Key atmospheric signatures for identifying the source reservoirs of volatiles in Uranus  
708 and Neptune. *Space Sci. Rev.* **216**, 77.
- 709 93. Ali-Dib M, Mousis O, Petit JM, Lunine JI. 2014 The measured compositions of Uranus and  
710 Neptune from their formation on the CO ice line. *Astrophys. J.* **793**, 1–7.
- 711 94. Panić O, Min M. 2017 Effects of disc mid-plane evolution on CO snowline location. *Mon. Not.*  
712 *R. Astron. Soc.* **467**, 1175–1–185.
- 713 95. Dodson-Robinson SE, Willacy K, Bodenheimer P, Turner NJ, Beichman CA. 2009 Ice lines,  
714 planetesimal composition and solid surface density in the solar nebula. *Icarus* **200**, 672–693.
- 715 96. Mousis O, Aguichine A, Helled R, Irwin P, Lunine J. 2020 The role of ice lines in the formation  
716 of Uranus and Neptune. *Phil. Trans. R. Soc. Lond. A* **current issue, under review**.
- 717 97. Brown ME. 2012 The compositions of Kuiper Belt Objects. *Annual Review of Earth and Planetary*  
718 *Sciences* **40**, 467–494.
- 719 98. Simonelli DP, Reynolds RT. 1989 The interiors of Pluto and Charon - structure, composition,  
720 and implications. *Geophys. Res. Lett.* **16**, 1209–1212.
- 721 99. Bierson CJ, Nimmo F. 2019 Using the density of Kuiper Belt Objects to constrain their  
722 composition and formation history. *Icarus* **326**, 10–17.
- 723 100. Hersant F, Gautier D, Lunine JI. 2004 Enrichment in volatiles in the giant planets of the Solar  
724 System. *Plan. & Space Sci.* **52**, 623–641.
- 725 101. Kunitomo M, Guillot T, Ida S, Takeuchi T. 2018 Revisiting the pre-main-sequence evolution of  
726 stars. II. Consequences of planet formation on stellar surface composition. *Astron. Astrophys.*  
727 **618**, A132.
- 728 102. Karkoschka E, Tomasko M. 2009 The haze and methane distributions on Uranus from HST-  
729 STIS spectroscopy. *Icarus* **202**, 287–309.
- 730 103. Sromovsky LA, Fry PM, Kim JH. 2011 Methane on Uranus: the case for a compact CH<sub>4</sub> cloud  
731 layer at low latitudes and a severe CH<sub>4</sub> depletion at high-latitudes based on re-analysis of  
732 Voyager occultation measurements and STIS spectroscopy. *Icarus* **215**, 292–312.
- 733 104. Orton GS, Moses JI, Fletcher LN, Mainzer AK, Hines D, Hammel HB, Martin-Torres J,  
734 Burgdorf M, Merlet C, Line MR. 2014 Mid-infrared spectroscopy of Uranus from the Spitzer  
735 infrared spectrometer: 2. Determination of the mean composition of the upper troposphere  
736 and stratosphere. *Icarus* **243**, 471–493.
- 737 105. Cavalié T, Moreno R, Lellouch E, Hartogh P, Venot O, Orton GS, Jarchow C, Encrenaz T, Selsis  
738 F, Hersant F, Fletcher LN. 2014 The first submillimeter observation of CO in the stratosphere  
739 of Uranus. *Astron. Astrophys.* **562**, A33.

- 1  
2  
3  
4  
5  
6  
7  
8  
9  
10  
11  
12  
13  
14  
15  
16  
17  
18  
19  
20  
21  
22  
23  
24  
25  
26  
27  
28  
29  
30  
31  
32  
33  
34  
35  
36  
37  
38  
39  
40  
41  
42  
43  
44  
45  
46  
47  
48  
49  
50  
51  
52  
53  
54  
55  
56  
57  
58  
59  
60
- 740 106. Guillot T. 2019 Uranus and Neptune are key to understand planets with hydrogen  
741 atmospheres. *arXiv e-prints* p. arXiv:1908.02092.
- 742 107. Niemann HB, Atreya SK, Carignan GR, Donahue TM, Haberman JA, Harpold DN, Hartle  
743 RE, Hunten DM, Kasprzak WT, Mahaffy PR, Owen TC, Way SH. 1998 The composition of the  
744 Jovian atmosphere as determined by the Galileo probe mass spectrometer. *J. Geophys. Res.* **103**,  
745 22831–22846.
- 746 108. Durante D, Parisi M, Serra D, Zannoni M, Notaro V, Racioppa P, Buccino DR, Lari G, Gomez  
747 Casajus L, Iess L, Folkner WM, Tommei G, Tortora P, Bolton SJ. 2020 Jupiter's gravity field  
748 halfway through the Juno mission. *Geophys. Res. Lett.* **47**, e86572.

For Review Only